NANO LETTERS

pubs.acs.org/NanoLett Letter

Double-Cavity Modulation of Exciton Polaritons in $CsPbBr_3$ Microwire

Zhe Zhang, Feilong Song, Zhenyao Li, Yuan-Fei Gao, Yu-Jia Sun, Wen-Kai Lou, Xinfeng Liu, Qing Zhang, Ping-Heng Tan, Kai Chang,* and Jun Zhang*

Cite This: *Nano Lett.* 2022, 22, 9365−9371 Read Online

ACCESS | Metrics & More | Article Recommendations | Supporting Information

ABSTRACT: The lead halide perovskite has become a promising candidate for the study of exciton polaritons due to their excellent optical properties. Here, both experimental and simulated results confirm the existence of two kinds of Fabry−Pérot microcavities in a single $CsPbBr_3$ microwire with an isosceles right triangle cross section, and we experimentally demonstrate that confined photons in a straight and a folded Fabry−Pérot microcavity are strongly coupled with excitons to form exciton polaritons. Furthermore, we reveal the polarization characteristic and double-cavity modulation of exciton polaritons emission by polarization-resolved fluorescence spectroscopy. Our results not only prove that the modulation of exciton polaritons emission can occur in this simple double-cavity system but also provide a possibility to develop related polariton devices.

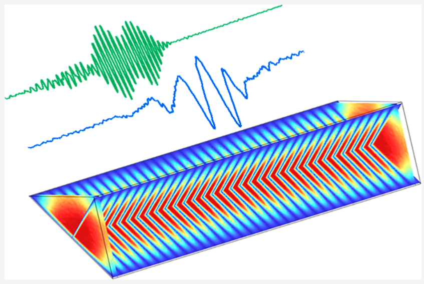

KEYWORDS: *$CsPbBr_3$ microwire, exciton polaritons, double Fabry−Pérot microcavity, polarization anisotropy*

Exciton polaritons (EPs), a kind of bosonic quasiparticle with a half-light and half-matter nature, are formed when excitons are strongly coupled with confined photons.[1] The confined photon and exciton dispersions anticross under strong coupling, resulting in two new eigenstates, termed the upper polariton branch (UPB) and the lower polariton branch (LPB), respectively. Compared with pure exciton systems, the half-light and half-matter nature of exciton polaritons provide the possibility to realize Bose−Einstein condensation (BEC) at much higher temperatures due to their extremely light-effective mass (of the order of 10^{-5} times the free-electron mass).[1−5] Their partially excitonic characteristic leads to strong polariton−polariton interactions, which enable the observation of superfluid phenomena in the polariton systems.[5,6] Over the past few years, there has been enormous and sustained interest in the use of lead halide perovskites to study lasing and BEC of EPs at room temperature due to its many excellent properties, including large exciton binding energy, high gain coefficient, and good photothermal stability.[7−9] Many intriguing phenomena, such as BEC,[10,11] exciton polariton laser,[10,12,13] long-range coherent exciton polariton condensed flow,[14] and all-optical switching,[15,16] have been realized in a $CsPbBr_3$ perovskite microcavity at room temperature. Furthermore, based on their crystalline anisotropy and strong photonic spin−orbit coupling (SOC), EPs in a $CsPbBr_3$ microcavity have been experimentally applied to opto-spintronics and topological photonics,[17−19] including optical switching between topologically nontrivial and trivial phases,[18] direct measurement of non-Hermitian topological invariants,[17] and the exciton-polariton condensed state with orthogonal polarization.[19]

The abundant morphology of $CsPbBr_3$ microstructures provides effective constraints on multidimensional light fields. $CsPbBr_3$ microstructures can form self-configuration microcavities during growth, which can be used as both a gain medium and an optical microcavity. The EPs in various self-configuration microcavities have been widely studied,[12,13,20−23] while the double-cavity modulation effect in a $CsPbBr_3$ microwire is not well-known. It is well-known that a double-cavity system will provide a promising avenue to construct new photonic devices, usually applied in the fields of the lasing modulation,[24,25] parity-time (PT) symmetry-based effects,[26,27] and quantum entanglement dynamics in a double-cavity system.[28,29]

In this paper, confined photons in both straight and folded Fabry−Pérot (F−P) microcavities can be strongly coupled with excitons to form exciton polaritons in the same $CsPbBr_3$ microwire. The double-cavity modulation of EPs induced by two types of self-configuration F−P microcavities is demonstrated by in situ photoluminescence (ISPL) and spatially resolved photoluminescence (SRPL) spectroscopy. Polarization-resolved photoluminescence spectroscopy reveals the polarization characteristic of exciton-polaritons emission due to the crystalline anisotropy. The numerical simulation of

Received: August 8, 2022
Revised: November 13, 2022
Published: November 18, 2022

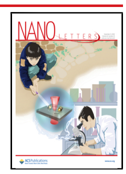

https://doi.org/10.1021/acs.nanolett.2c03147
Nano Lett. 2022, 22, 9365−9371

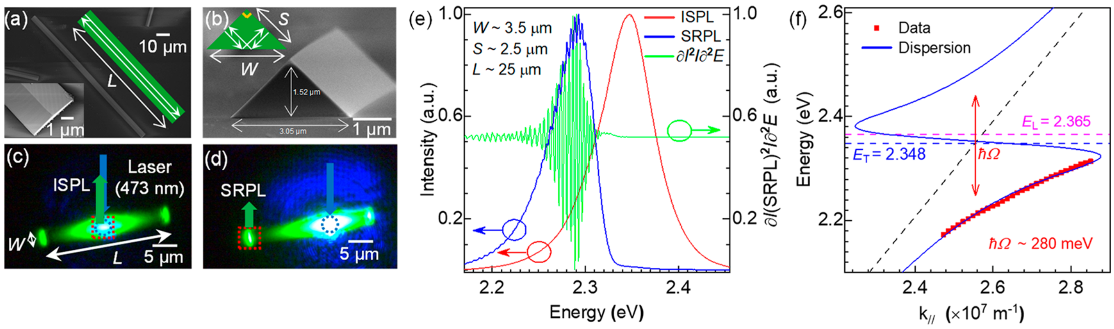

Figure 1. Optical characterization of $CsPbBr_3$ microwires and dispersion relationship of EPs in a straight F−P microcavity. (a) SEM image of a single $CsPbBr_3$ microwire on a mica substrate. The illustration shows that the F−P microcavity can be formed along the L direction. The lower left inset shows the zoom-in view of the end facet of the microwire. (b) SEM image of the end facet of a single $CsPbBr_3$ microwire observed from the vertical end facet direction after 3 months. The illustration is a folded F−P microcavity formed between its two isosceles right triangle side walls of the microwire. The S is the side length of an isosceles right triangle, and the W is the length of the hypotenuse. (c, d) The ISPL and SRPL spectrum measurement setup. ISPL refers that the collection point of the PL signal is the same as the excitation point, while SRPL means that the collection point of the PL signal is different from the excitation point. The blue and green arrows show the direction of the laser excitation and fluorescence collection, respectively. (e) ISPL spectrum (red line), SRPL spectrum (blue line), and 2^{nd}-SRPL spectrum (green line). (f) The dispersion relationship of EPs based on the SRPL spectrum in panel e.

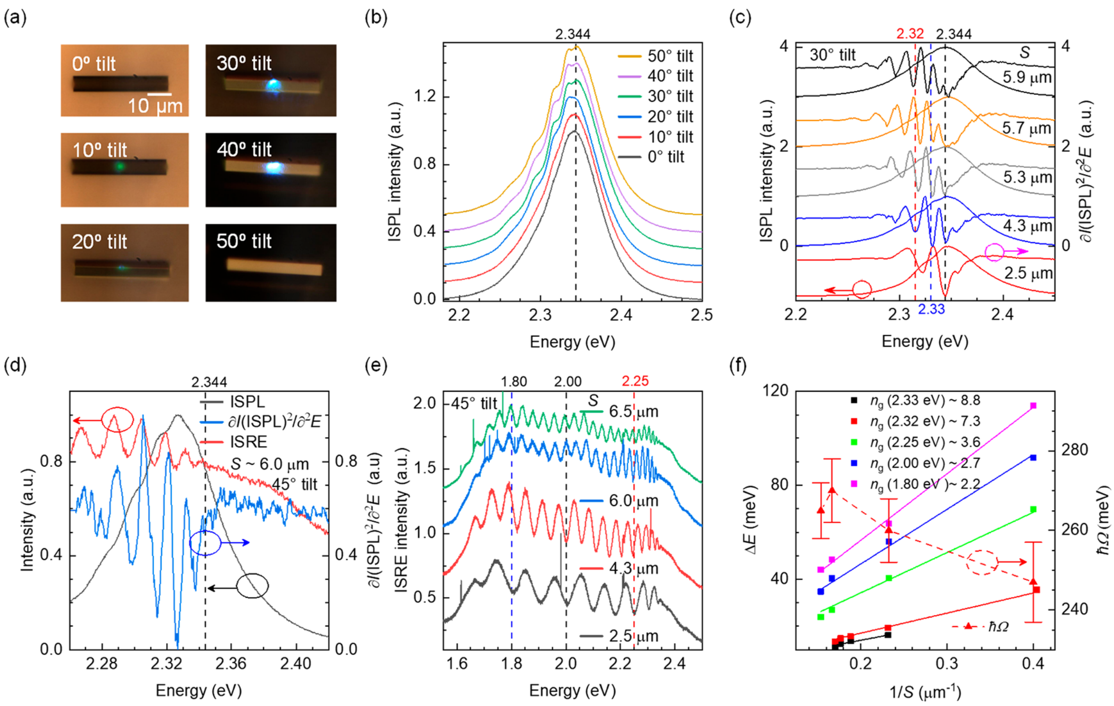

Figure 2. Optical characterization of $CsPbBr_3$ microwires and dispersion relationship of EPs in a folded F−P microcavity. (a) Optical micrographs of a single $CsPbBr_3$ microwire at different tilt angles. The value of the angle represents the angle between the incident light and the substrate normal. (b) ISPL spectra of a single $CsPbBr_3$ microwire at different tilt angles in panel a. (c) ISPL and their 2^{nd}-ISPL spectra with different side lengths S at a 30° tilt. (d) ISPL spectrum, ISRE spectrum, and 2^{nd}-ISPL spectrum in a single $CsPbBr_3$ microwire with side length $S \sim 6.0\ \mu m$ at a 45° tilt. (e) ISRE spectra of four $CsPbBr_3$ microwires with different side lengths at a 45° tilt. (f) ΔE and $\hbar\Omega$ of a folded F−P microcavity vary with the inverse of side length $1/S$ at a 45° tilt.

resonant frequencies, field distributions, and quality factors of F−P cavity modes agree well with the experimental results under TE and TM polarization directions. Our results provide a considerable prospect for the practical applications of an all-inorganic lead halide perovskite and all-optical polaritonic devices at room temperature.

The $CsPbBr_3$ microwires with an isosceles right triangle cross section were grown on a mica substrate by a chemical vapor deposition (CVD) method (see Methods). The scanning electron microscopy (SEM) images in Figure 1a,b show that a single $CsPbBr_3$ microwire on a mica substrate has an isosceles triangular prism shape, and its smooth surface indicates that the material crystallizes well during growth. The $CsPbBr_3$ microwire has a good optical stability and crystalline quality in the atmosphere (Figure 1S), making them attractive for real-world application.[30] Because the cross-section of this kind of $CsPbBr_3$ microwire is an isosceles right triangle (Figure 1b), the geometric configuration of this kind of $CsPbBr_3$ microwire can form two types of F−P microcavities, one straight F−P microcavity is formed along the longitudinal length (i.e., L) of the $CsPbBr_3$ microwire, and the other folded F−P microcavity is formed between its two isosceles right

https://doi.org/10.1021/acs.nanolett.2c03147
Nano Lett. 2022, 22, 9365−9371

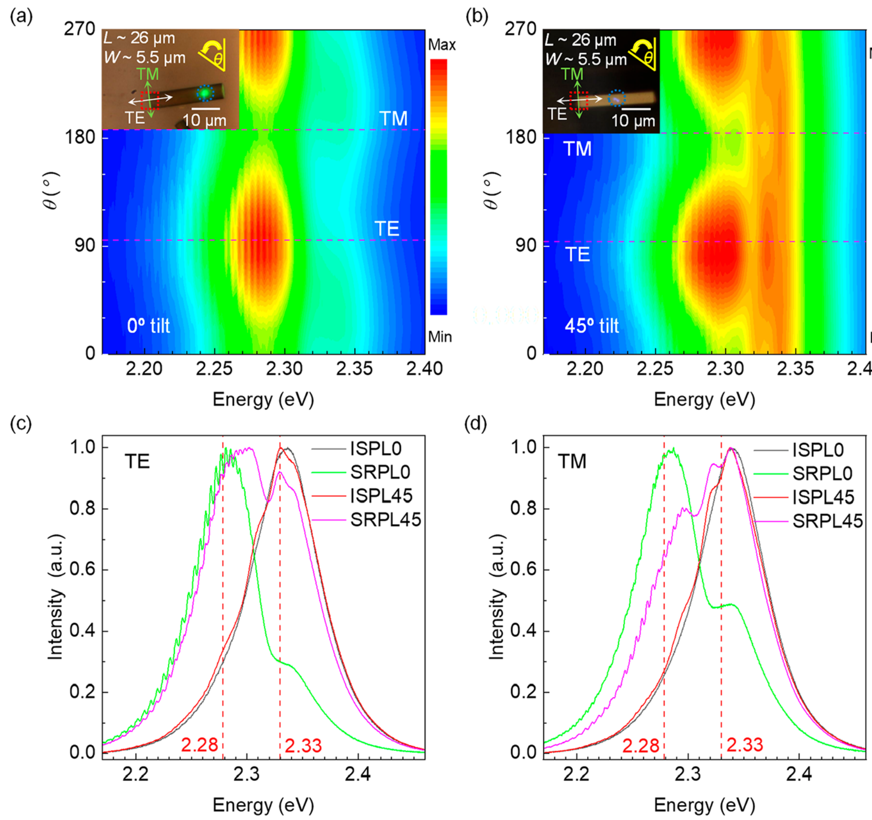

Figure 3. Polarization-resolved PL spectra of a single $CsPbBr_3$ microwire at two different tilting angles. (a, b) Pseudocolor map of SRPL spectra of a single $CsPbBr_3$ microwire at 0° and 45° tilts, respectively. The illustration shows the optical micrograph and polarization collection configuration. The θ is the rotation angle of the fast axis of the linear polarizer. We are specifying that the initial vertical direction is $\theta = 0$. (c, d) ISPL and SRPL spectra under TE and TM polarization directions, respectively. SRPL0 and SRPL45 represent the SRPL spectra of the sample at 0° and 45° tilts, respectively. The same notation applies to ISPL0 and ISPL45.

triangle side walls (i.e., S), as shown in Figure 1a,b, respectively. The folded cavity formed by the total reflection from two isosceles right triangle side walls is not considered here. The field distributions inside a single $CsPbBr_3$ microwire simulated by a finite element method software (COMSOL Multiphysics) indicate that the two types of microcavities can exist (Figure S2). Next, we will explore the formation of these two types of microcavities and the strong coupling between the two types of confined photons and excitons, respectively. First, we study the EPs in a straight F−P microcavity. Figure 1c,d shows how the sample is excited and collected for the ISPL and SRPL measurements, respectively. Figure 1e shows the ISPL and SRPL spectra of the $CsPbBr_3$ microwire with longitudinal length $L \sim 25$ μm on a mica substrate. The peak energy of the ISPL spectrum corresponds to the transverse exciton energy (i.e., $E_T \sim 2.348$ eV), as shown by the red curve in Figure 1e. The SRPL spectrum has a series of oscillation peaks as shown by the blue curve in Figure 1e. To obtain the oscillation peak values more quickly and accurately, we use the second derivative spectrum of SRPL (i.e., 2^{nd}-SRPL) spectrum, in which each dip of the 2^{nd}-SRPL spectrum (green curve in Figure 1e) indicates one oscillation peak of the original SRPL spectrum. Compared to the common fitting methods, the 2^{nd}-SRPL spectroscopy can resolve weaker oscillation peaks. The asymmetry line-shape of ISPL spectrum is attributed to self-absorption induced by Urbach tail states,[20] while the low energy oscillation peaks of SRPL spectrum are attributed to light reabsorption or/and inelastic scattering processes (Figure S3).[20,22] The $E-k_{//}$ dispersion relationship of EPs can be obtained through the dielectric function model (see Methods).[12,13,20−22,31] Figure 1f shows the dispersion relationship of the EPs in the straight F−P microcavity acquired from Figure 1e. The red squares are experimental data, and the solid blue line is the theoretical dispersion curve. From the fitting of the data, we extracted the Rabi splitting energy (i.e., $\hbar\Omega$) of 280 meV, which is much higher than the dissipation energy of excitons and cavity photons (i.e., $\hbar\gamma_{ex} \sim 70$ meV, $\hbar\gamma_{ph} \sim 15$ meV). Considering the damping relation $\hbar\Omega/2\{\hbar\gamma_{ex}, \hbar\gamma_{ph}\} > 1$, we can confirm that this system is in the strong-coupling regime.[3,12,32]

The cross section of the single $CsPbBr_3$ microwire is an isosceles right triangle, which is difficult to form a stable whispering gallery mode (WGM) due to the leakage of propagating photons.[33] A folded F−P cavity can be formed by partial reflection from two right-angle side walls and total reflection from the bottom wall, as shown in Figure 1b. However, the strong coupling between confined photons and excitons in this kind of self-configuration folded F−P microcavity has been seldom studied in $CsPbBr_3$. Figure 2a exhibits the optical micrographs of a single $CsPbBr_3$ microwire at different tilt angles. By tilting the microwire, the obvious cavity modes can be observed when the tilt angle is 30−50° as shown in Figure 2b. Then, we measured the ISPL spectra from the side of samples with different S values at a 30° tilt, as shown in Figure 2c. Here, the geometrical optical path length (i.e., equal to the side length S) of the folded F−P cavity has a fixed relationship with the width (i.e., W) of the hypotenuse of a right triangle, namely $W = \sqrt{2}\ S$, as shown in Figure 1b. To

https://doi.org/10.1021/acs.nanolett.2c03147
Nano Lett. 2022, 22, 9365−9371

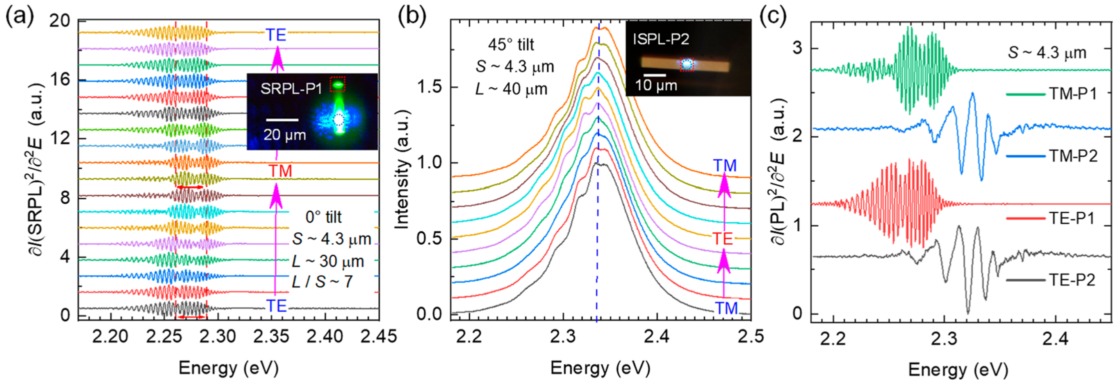

Figure 4. Polarization-related PL and 2nd-PL spectra of a straight and folded F−P microcavity. (a) Polarization-dependent 2nd-SRPL spectra of a straight F−P microcavity at a 0° tilt. The inset shows the fluorescence image of the sample (labeled P1). The inset red dotted line square is the collection position, and the blue dotted line circle is the excitation position. One of the wave packets of 2nd-SRPL spectral envelope in TE polarization modes is sandwiched between the two red dashed lines. (b) Polarization-resolved ISPL spectra of a folded F−P microcavity at a 45° tilt. The inset shows the fluorescence image of the microwire (labeled P2). (c) Polarization-resolved 2nd-SRPL spectra in P1 and polarization-resolved 2nd-ISPL spectra in P2 under TM and TE polarization directions, respectively. The figure gives information about the *S* and *L* of P1 and P2, respectively.

avoid the influence of the straight F−P cavity, we choose the measured microwire with rough end facets or place the acquisition area away from the end facet of the microwire (Figure S4). Since the mica substrate is tilted more than 30°, the white light reflected from the mica substrate can hardly enter the objective lens. Here, the in situ reflection (i.e., ISRE) spectrum referred to here and later are represented by the normalized intensity of reflected light. We can see that the oscillation peaks of ISRE spectrum are very well consistent with the oscillation peaks of the second-ISPL spectrum, which provides another evidence of the existence of folded F−P cavity, as shown in Figure 2d. Figure 2e displays the ISRE spectra of the $CsPbBr_3$ microwires with different side lengths *S* at a 45° tilt. The exciting light is just perpendicular to the side face of the microwire and the reflection signal from the mica substrate is very weak. We can see that the cavity mode spacing (i.e., ΔE) increases with the decrease of the *S*. Figure 2f shows that the ΔE near the energy labeled by the dashed line in Figure 2c,e is linearly related to $1/S$, which indicates that this type of microcavity is a kind of F−P cavity. Based on the group refractive index (i.e., n_g) formula near a certain energy $\Delta E = hc/(2n_gS)$,[8,34] the n_g increases from 2.2 to 8.8 with the increase of the energy from 1.80 to 2.33 eV. The variation law of the n_g is consistent with the dispersion relationship of exciton polaritons. The change of the n_g with energy can be used to study slow light.[20] The $\hbar\Omega$ of the four microwires in Figure 2e can be obtained by using the coupled oscillator model, as shown in the red triangle in Figure 2f. Since the microcavities are micrometer size, the $\hbar\Omega$ of EPs is close to that of bulk material (i.e., $\hbar\Omega_{bulk}$), about 250−270 meV. The uncertainty of Rabi splitting $\hbar\Omega$ in Figure 2f results from uncertainty in the wavevector of the lowest energy mode (i.e., the fitting parameter k_0).

At room temperature, the orthogonal lattice structure[8,19,35] of $CsPbBr_3$ will introduce birefringence, which results in X−Y splitting (related to crystalline anisotropy) of the exciton-polariton states.[17,19,36] This phenomenon can be uncovered by optical polarization characterization of EPs. The polarization properties of exciton polaritons in this work are studied by using confocal polarization-resolved photoluminescence spectroscopy. Figure 3a shows the polarization-resolved SRPL0 spectra of a single $CsPbBr_3$ microwire at a 0° tilt, where the collected light is perpendicular to the substrate. The TE polarization is specified along the *L* direction, as shown in the inset of Figure 3a,b. To quantitatively describe the linear polarization characteristic of EPs emission, the polarization degree *P* is defined as $P = (I_{max} - I_{min})/(I_{max} + I_{min})$. Here, I_{max} and I_{min} are the maximum and minimum intensity of the polarization-resolved SRPL spectra, respectively. Emission anisotropy with the $P \approx 25\%$ between 2.16 and 2.30 eV is demonstrated in the microwires with $W > 140$ nm due to the electrostatic dielectric confinement.[37] Meanwhile, the polarization direction of the emission light is related to the geometric structure, and the emission intensity along the longitudinal *L* direction is stronger than that along the transverse *W* direction. Polarization-resolved anisotropy can be quantitatively explained by the large dielectric difference between the $CsPbBr_3$ microwire and the surrounding environment, and the *P* is related to the diffraction-related multi-waveguide mode competition.[37] Similarly, Figure 3b shows the SRPL45 spectra of this $CsPbBr_3$ microwire at a 45° tilt results in similar polarization characteristics as shown in Figure 3a. From the photoluminescence (i.e., PL) spectra of two different polarization modes in Figure 3c,d, the SRPL45 spectra have a double-cavity modulated pattern. One is induced by a straight F−P cavity as shown in SRPL0 spectra, and the other is from a folded F−P cavity as shown in ISPL45 spectra. To our best knowledge, this kind of double-cavity modulated EPs has never been reported yet. Due to the influence of measurement method, the polarization-resolved energy movement detected here is mainly related to crystalline anisotropy.[17−19] Because the multicavity mode information mainly comes from the diffraction effect of the end facet of the straight F−P cavity in SRPL0 spectra, it is not easy to distinguish the change of the peak position of the cavity mode from the polarization. However, and the peak energy under TE polarization in ISPL0 spectrum is about 4 meV smaller than that under TM polarization (Figure S5a), and the peak position of cavity mode in ISPL45 spectrum changes significantly with polarization (Figure S5b). Therefore, the orthogonal lattice structure of $CsPbBr_3$ will exhibit optical anisotropy.[38] Lu et al. confirmed that the crystal structure of $CsPbBr_3$ micro/nanowires is an orthorhombic phase.[35] It is similar to Rydberg exciton polaritons in the $CsPbBr_3$ perovskite cavity reported by Bao

https://doi.org/10.1021/acs.nanolett.2c03147
Nano Lett. 2022, 22, 9365−9371

et al.,[38] which indicates that X−Y splitting plays a key role. This is consistent with the X−Y splitting of the exciton-polariton states observed in traditional planar microcavities.[17,19,36,38] This makes it possible to achieve polarization-modulated EPs lasing and EPs BEC in this $CsPbBr_3$ micro/nanowires.

To further explore the correlation between two types of F−P microcavities, two $CsPbBr_3$ microwires with the same S but different L were chosen (Figure 4a,b). Figure 4a shows the spectral envelopes of polarization-resolved 2nd-SRPL spectra are modulated by a folded F−P microcavity. This modulation effect is related to the aspect ratio L/S. The L/S is ∼7 in Figure 4a, and the $L/S \sim 9$ in Figure 4b. Figures S6 and S7 shows the field distribution and corresponding wavelength of the same order cavity mode, which is consistent with the experimental results. This further confirms the existence of a double-cavity. Figure S8a,b shows that the ratio of the mode spacing between the folded cavity and the straight cavity is almost equal to the number of cavity modes of the straight cavity contained in the adjacent folded cavity mode, which is close to the cavity length ratio $L/S \sim 7$. The quality factor Q of each cavity mode was obtained by multipeak fitting of the spectrum (Figure S8c). The Q of the straight F−P microcavity is about three times larger than that of the folded F−P microcavity (Figure S8d). From Figures S8d and S9, there is an optimized wavelength range and cavity modes have the highest Q-factor. The quality factor Q of the cavity mode is affected by cavity loss (i.e., light escapes at the boundary) and media loss (i.e., light is absorbed by the media), which lead to an optimized wavelength range for EPs modes. The simulation result with media loss and cavity loss considered is in good agreement with the experimental results (Figure S9). Due to the competition between cavity losses and dielectric losses, there will be an optimized wavelength range in which the quality factor of the resonant mode is highest.[39] In our simulations, the refractive index is a function of energy,[20,30] and the mica has a refractive index of 1.6.[33] Despite the differences in the optimal quality factors Q of the two microcavities, the spectra observed at the end facet can still carry the signals of the two kinds of F−P cavities, which may indicate that double-cavity modulation associated with mode competition can be achieved in SRPL spectral measurements (Figure 3 and Figure S3). The mode competition between the two Fabry−Pérot cavities may be more evident when stimulated radiation occurs, which needs further study. Figure 4c gives the polarization-resolved 2nd-SRPL spectra of P1 and the polarization-resolved second-ISPL spectra of P2, and the two types of polarization modes do modulate each other in the energy overlap region. This optical modulation may be carried out by changing the cavity length ratio and the optimized wavelength range of two types of F−P microcavities. The difference between optical gain and loss may provide a powerful platform for testing various theoretical proposals regarding PT symmetry.[26,27]

In conclusion, both experimental and simulated results confirm the existence of two kinds of F−P cavities, and two types of microcavity photons (i.e., one is a straight F−P microcavity and the other is a folded F−P microcavity) can be strongly coupled with excitons to form exciton polaritons in the same $CsPbBr_3$ micowire. The crystalline anisotropy is observed from polarization-resolved PL spectra. We present the numerical simulation of resonant frequencies, field distributions, and quality factors of F−P cavity modes under TE and TM polarization directions, which agree well with the experimental results. Besides, we found that there is a double-cavity modulation phenomenon of EPs emission in a single $CsPbBr_3$ microwire according to the second derivative spectrum of the PL spectrum. These results indicate that the $CsPbBr_3$ microwire structure is a good platform for studying novel optical modulation behavior and optical devices of EPs.

■ METHODS

Sample CVD Growth. $CsPbBr_3$ microwires were grown on a mica substrate by a single furnace CVD method. Mixed CsBr and $PbBr_2$ powders with a molar ratio of 2:1 as a precursor were placed in the center of the quartz tube. The freshly cleaved mica was cleaned with an acetone solution for 10 min and put inside the downstream of the quartz tube. The distance between the mica substrate and precursor was 10 cm. First, a large amount of argon gas was pumped to expel the air in the quartz tube, and then the flow rate of argon gas was kept at 60 sccm. The quartz tube was heated from room temperature to 550 °C for 30 min. The temperature inside the quartz tube was stabilized at 550 °C for 10 min. After the synthesis, the tube was cooled down naturally.

Optical Spectroscopy Characterization. The morphology of $CsPbBr_3$ microwires was characterized by field emission scanning electron microscopy (Hitachi S4800). SmartRaman confocal-micro-Raman module was used for photoluminescence measurement and microscopic imaging with a 100× objective lens (NA = 0.60) under the backscattering geometry. The module was developed by Institute of Semiconductors,Chinese Academy of Sciences, which is coupled with a Horiba iHR550 spectrometer and a charge-coupled device (CCD) detector. The optical and fluorescence images were obtained by illuminating $CsPbBr_3$ microwires with a halogen lamp and 473 nm laser, respectively. PL spectra measurements were performed with a continuous 473 nm linearly polarized laser. After passing through a 473 nm bandpass filter, the fluorescence of the microwire entered the spectrometer (Horiba iHR550) and a CCD detector through the same microscope objective. Based on the same measurement configuration, the reflection spectra were measured by changing the laser to the white light source. If polarization measurement is made, a half-wave plate and a Glan Taylor prism were added as a polarizer between the microscope objective and the spectrometer. To improve the spatial resolution, a confocal system was placed on the collecting path. All tests were performed at room temperature.

Dielectric Function Model. To explore the strong interaction between excitons and confined photons in the $CsPbBr_3$ microwires, the EPs dispersion relationship was studied according to the classical Lorentz oscillator coupling model. As shown in the following formula[12,13,20−22,31,40]

$$E(k_{//}) = \frac{\hbar c k_{//}}{\sqrt{\varepsilon_b\left(1 + \frac{E_L^2 - E_T^2}{E_T^2 - E^2 - iE\hbar\gamma}\right)}}$$

Here, E_L is the longitudinal exciton energy, E_T is the transverse exciton energy, ε_b is the background dielectric constant, γ is the damping constant, $k_{//}$ is the wave vector, and c is the speed of light in a vacuum. E is the central energy of the oscillation peak in the SRPL spectrum or the ISPL45 spectrum with cavity mode information, and E_T takes the central energy of the ISPL0 spectrum without cavity mode information. In this paper, we use the reported[20] ε_b = 4.6 for fitting. $\hbar\gamma$ is

https://doi.org/10.1021/acs.nanolett.2c03147
Nano Lett. 2022, 22, 9365−9371

determined by the full width at half-maximum (fwhm) of the ISPL0 spectrum. The wave vector $k_{//} = k_0 + n\pi/L$ (n = 1, 2, 3, ...), L is the geometrical length of the resonator (e.g., the longitudinal length L or the side length S), and the k_0 is the adjustable initial wave vector to account for the absence of knowledge on the wavevector of the lowest energy mode.[20,31] When the cavity photons and excitons come close to resonance, it causes the exciton level to split, called Rabi splitting (i.e., $\hbar\Omega$). The minimum vertical distance between UPB and LPB on the EPs dispersion curve can be used to estimate the $\hbar\Omega$ of the system. Since the microwires studied close to bulk materials, $\hbar\Omega$ can be approximated as $\hbar\Omega_{\text{bulk}} \sim \sqrt{2E_T E_{LT}}$, $E_{LT} = E_L - E_T$.

■ ASSOCIATED CONTENT

Supporting Information

The Supporting Information is available free of charge at https://pubs.acs.org/doi/10.1021/acs.nanolett.2c03147.

Additional information on sample stability, optical micrograph of the sample, characterization of photoluminescence at room temperature, and simulation of quality factor and field distribution for cavity mode (PDF)

■ AUTHOR INFORMATION

Corresponding Authors

Kai Chang − *State Key Laboratory of Superlattices and Microstructures, Institute of Semiconductors, Chinese Academy of Sciences, Beijing 100083, China; Center of Materials Science and Optoelectronics Engineering, University of Chinese Academy of Sciences, Beijing 100049, China;* Email: kchang@semi.ac.cn

Jun Zhang − *State Key Laboratory of Superlattices and Microstructures, Institute of Semiconductors, Chinese Academy of Sciences, Beijing 100083, China; Center of Materials Science and Optoelectronics Engineering, University of Chinese Academy of Sciences, Beijing 100049, China;* orcid.org/0000-0002-9831-6796; Email: zhangjwill@semi.ac.cn

Authors

Zhe Zhang − *State Key Laboratory of Superlattices and Microstructures, Institute of Semiconductors, Chinese Academy of Sciences, Beijing 100083, China; Center of Materials Science and Optoelectronics Engineering, University of Chinese Academy of Sciences, Beijing 100049, China*

Feilong Song − *State Key Laboratory of Superlattices and Microstructures, Institute of Semiconductors, Chinese Academy of Sciences, Beijing 100083, China; Beijing Academy of Quantum Information Science, Beijing 100193, China*

Zhenyao Li − *State Key Laboratory of Superlattices and Microstructures, Institute of Semiconductors, Chinese Academy of Sciences, Beijing 100083, China; Center of Materials Science and Optoelectronics Engineering, University of Chinese Academy of Sciences, Beijing 100049, China*

Yuan-Fei Gao − *Beijing Academy of Quantum Information Science, Beijing 100193, China;* orcid.org/0000-0001-5455-5421

Yu-Jia Sun − *State Key Laboratory of Superlattices and Microstructures, Institute of Semiconductors, Chinese Academy of Sciences, Beijing 100083, China; Center of Materials Science and Optoelectronics Engineering, University of Chinese Academy of Sciences, Beijing 100049, China*

Wen-Kai Lou − *State Key Laboratory of Superlattices and Microstructures, Institute of Semiconductors, Chinese Academy of Sciences, Beijing 100083, China; Center of Materials Science and Optoelectronics Engineering, University of Chinese Academy of Sciences, Beijing 100049, China;* orcid.org/0000-0001-6906-6479

Xinfeng Liu − *CAS Key Laboratory of Standardization and Measurement for Nanotechnology, CAS Center For Excellence in Nanoscience, National Center for Nanoscience and Technology, Beijing 100190, China;* orcid.org/0000-0002-7662-7171

Qing Zhang − *Department of Materials Science and Engineering, College of Engineering, Peking University, Beijing 100871, China;* orcid.org/0000-0002-6869-0381

Ping-Heng Tan − *State Key Laboratory of Superlattices and Microstructures, Institute of Semiconductors, Chinese Academy of Sciences, Beijing 100083, China; Center of Materials Science and Optoelectronics Engineering, University of Chinese Academy of Sciences, Beijing 100049, China;* orcid.org/0000-0001-6575-1516

Complete contact information is available at: https://pubs.acs.org/10.1021/acs.nanolett.2c03147

Author Contributions

J.Z. and K.C. led the project. Z.Z. produced the samples and performed spectroscopy. F.S. constructed the optical setup. F.S., Y.G., and Y.S. assisted in spectral testing. Z.Z. and Z.L. performed optical simulations. Z.Z. and J.Z. analyzed the data and wrote the paper. All the authors discussed the results and revised the paper.

Notes

The authors declare no competing financial interest.

■ ACKNOWLEDGMENTS

Authors acknowledge the funding support from National Key Research and Development Program of China (2017YFA0303401, 2018YFA0306101), CAS Interdisciplinary Innovation Team, National Natural Science Foundation of China (12074371, 11974340, and 92265203), and Strategic Priority Research Program of Chinese Academy of Sciences (XDB28000000). We thank H.C. for his help.

■ REFERENCES

(1) Kasprzak, J.; Richard, M.; Kundermann, S.; Baas, A.; Jeambrun, P.; Keeling, J. M.; Marchetti, F. M.; Szymanska, M. H.; Andre, R.; Staehli, J. L.; Savona, V.; Littlewood, P. B.; Deveaud, B.; Dang, L. S. Bose−Einstein condensation of exciton polaritons. *Nature* **2006**, *443* (7110), 409−414.

(2) Balili, R.; Hartwell, V.; Snoke, D.; Pfeiffer, L.; West, K. Bose−Einstein condensation of microcavity polaritons in a trap. *Science* **2007**, *316* (5827), 1007−1010.

(3) Deng, H.; Haug, H.; Yamamoto, Y. Exciton-polariton Bose−Einstein condensation. *Rev. Mod. Phys.* **2010**, *82* (2), 1489−1537.

(4) Byrnes, T.; Kim, N. Y.; Yamamoto, Y. Exciton−polariton condensates. *Nat. Phys.* **2014**, *10* (11), 803−813.

(5) Amo, A.; Lefrère, J.; Pigeon, S.; Adrados, C.; Ciuti, C.; Carusotto, I.; Houdré, R.; Giacobino, E.; Bramati, A. Superfluidity of polaritons in semiconductor microcavities. *Nat. Phys.* **2009**, *5* (11), 805−810.

(6) Lagoudakis, K. G.; Wouters, M.; Richard, M.; Baas, A.; Carusotto, I.; André, R.; Dang, L. S.; Deveaud-Plédran, B. Quantized

vortices in an exciton−polariton condensate. *Nat. Phys.* **2008**, *4* (9), 706−710.
(7) Zhang, Q.; Shang, Q.; Su, R.; Do, T. T. H.; Xiong, Q. Halide Perovskite Semiconductor Lasers: Materials, Cavity Design, and Low Threshold. *Nano Lett.* **2021**, *21* (5), 1903−1914.
(8) Zhang, Q.; Su, R.; Liu, X.; Xing, J.; Sum, T. C.; Xiong, Q. High-Quality Whispering-Gallery-Mode Lasing from Cesium Lead Halide Perovskite Nanoplatelets. *Adv. Funct. Mater.* **2016**, *26* (34), 6238−6245.
(9) Su, R.; Fieramosca, A.; Zhang, Q.; Nguyen, H. S.; Deleporte, E.; Chen, Z.; Sanvitto, D.; Liew, T. C. H.; Xiong, Q. Perovskite semiconductors for room-temperature exciton-polaritonics. *Nat. Mater.* **2021**, *20* (10), 1315−1324.
(10) Su, R.; Diederichs, C.; Wang, J.; Liew, T. C. H.; Zhao, J.; Liu, S.; Xu, W.; Chen, Z.; Xiong, Q. Room-Temperature Polariton Lasing in All-Inorganic Perovskite Nanoplatelets. *Nano Lett.* **2017**, *17* (6), 3982−3988.
(11) Su, R.; Ghosh, S.; Wang, J.; Liu, S.; Diederichs, C.; Liew, T. C. H.; Xiong, Q. Observation of exciton polariton condensation in a perovskite lattice at room temperature. *Nat. Phys.* **2020**, *16* (3), 301−306.
(12) Shang, Q.; Li, M.; Zhao, L.; Chen, D.; Zhang, S.; Chen, S.; Gao, P.; Shen, C.; Xing, J.; Xing, G.; Shen, B.; Liu, X.; Zhang, Q. Role of the Exciton-Polariton in a Continuous-Wave Optically Pumped CsPbBr3 Perovskite Laser. *Nano Lett.* **2020**, *20* (9), 6636−6643.
(13) Du, W.; Zhang, S.; Shi, J.; Chen, J.; Wu, Z.; Mi, Y.; Liu, Z.; Li, Y.; Sui, X.; Wang, R.; Qiu, X.; Wu, T.; Xiao, Y.; Zhang, Q.; Liu, X. Strong Exciton−Photon Coupling and Lasing Behavior in All-Inorganic CsPbBr3Micro/Nanowire Fabry-Pérot Cavity. *ACS Photonics* **2018**, *5* (5), 2051−2059.
(14) Su, R.; Wang, J.; Zhao, J.; Xing, J.; Zhao, W.; Diederichs, C.; Liew, T.; Xiong, Q. Room temperature long-range coherent exciton polariton condensate flow in lead halide perovskites. *Sci. Adv.* **2018**, *4* (10), eaau0244.
(15) Feng, J.; Wang, J.; Fieramosca, A.; Bao, R.; Zhao, J.; Su, R.; Peng, Y.; Liew, T.; Sanvitto, D.; Xiong, Q. All-optical switching based on interacting exciton polaritons in self-assembled perovskite microwires. *Sci. Adv.* **2021**, *7* (46), eabj6627.
(16) Zhang, J.; Zhang, Q. All-optical switching based on self-assembled halide perovskite microwires. *J. Semicond.* **2022**, *43* (1), 010401.
(17) Su, R.; Estrecho, E.; Bieganska, D.; Huang, Y.; Wurdack, M.; Pieczarka, M.; Truscott, A. G.; Liew, T. C. H.; Ostrovskaya, E. A.; Xiong, Q. Direct measurement of a non-Hermitian topological invariant in a hybrid light-matter system. *Sci. Adv.* **2021**, *7* (45), eabj8905.
(18) Su, R.; Ghosh, S.; Liew, T. C. H.; Xiong, Q. Optical switching of topological phase in a perovskite polariton lattice. *Sci. Adv.* **2021**, *7* (21), eabf8049.
(19) Spencer, M. S.; Fu, Y. P.; Schlaus, A. P.; Hwang, D.; Dai, Y. A.; Smith, M. D.; Gamelin, D. R.; Zhu, X. Y. Spin-orbit−coupled exciton-polariton condensates in lead halide perovskites. *Sci. Adv.* **2021**, *7* (49), eabj7667.
(20) Shang, Q.; Li, C.; Zhang, S.; Liang, Y.; Liu, Z.; Liu, X.; Zhang, Q. Enhanced Optical Absorption and Slowed Light of Reduced-Dimensional CsPbBr3 Nanowire Crystal by Exciton-Polariton. *Nano Lett.* **2020**, *20* (2), 1023−1032.
(21) Park, K.; Lee, J. W.; Kim, J. D.; Han, N. S.; Jang, D. M.; Jeong, S.; Park, J.; Song, J. K. Light-Matter Interactions in Cesium Lead Halide Perovskite Nanowire Lasers. *J. Phys. Chem. Lett.* **2016**, *7* (18), 3703−3710.
(22) Zhao, Z.; Zhong, M.; Zhou, W.; Peng, Y.; Yin, Y.; Tang, D.; Zou, B. Simultaneous Triplet Exciton−Phonon and Exciton−Photon Photoluminescence in the Individual Weak Confinement CsPbBr3Micro/Nanowires. *J. Phys. Chem. C* **2019**, *123* (41), 25349−25358.
(23) Han, Q.; Wang, J.; Lu, J.; Sun, L.; Lyu, F.; Wang, H.; Chen, Z.; Wang, Z. Transition Between Exciton-Polariton and Coherent Photonic Lasing in All-Inorganic Perovskite Microcuboid. *ACS Photonics* **2020**, *7* (2), 454−462.
(24) Zhang, C.; Zou, C.; Dong, H.; Yan, Y.; Yao, J.; Zhao, Y. Dual-color single-mode lasing in axially coupled organic nanowire resonators. *Sci. Adv.* **2017**, *3* (7), e1700225.
(25) Du, Y.; Zou, C.-L.; Zhang, C.; Wang, K.; Qiao, C.; Yao, J.; Zhao, Y. S. Tuneable red, green, and blue single-mode lasing in heterogeneously coupled organic spherical microcavities. *Light: Sci. Appl.* **2020**, *9* (1), 151.
(26) Chang, L.; Jiang, X.; Hua, S.; Yang, C.; Wen, J.; Jiang, L.; Li, G.; Wang, G.; Xiao, M. Parity−time symmetry and variable optical isolation in active−passive-coupled microresonators. *Nat. Phys.* **2014**, *8* (7), 524−529.
(27) Peng, B.; Özdemir, Ş. K.; Lei, F.; Monifi, F.; Gianfreda, M.; Long, G. L.; Fan, S.; Nori, F.; Bender, C. M.; Yang, L. Parity−time-symmetric whispering-gallery microcavities. *Nat. Phys.* **2014**, *10* (5), 394−398.
(28) Chen, Z. X.; Lin, Q.; He, B.; Lin, Z. Y. Entanglement dynamics in double-cavity optomechanical systems. *Opt. Express* **2017**, *25* (15), 17237−17248.
(29) Pinard, M.; Dantan, A.; Vitali, D.; Arcizet, O.; Briant, T.; Heidmann, A. Entangling movable mirrors in a double-cavity system. *Europhys. Lett.* **2005**, *72* (5), 747−753.
(30) Eaton, S. W.; Lai, M.; Gibson, N. A.; Wong, A. B.; Dou, L.; Ma, J.; Wang, L. W.; Leone, S. R.; Yang, P. Lasing in robust cesium lead halide perovskite nanowires. *Proc. Natl. Acad. Sci. U. S. A.* **2016**, *113* (8), 1993−1998.
(31) Shang, Q.; Zhang, S.; Liu, Z.; Chen, J.; Yang, P.; Li, C.; Li, W.; Zhang, Y.; Xiong, Q.; Liu, X.; Zhang, Q. Surface Plasmon Enhanced Strong Exciton-Photon Coupling in Hybrid Inorganic-Organic Perovskite Nanowires. *Nano Lett.* **2018**, *18* (6), 3335−3343.
(32) Evans, T. J. S.; Schlaus, A.; Fu, Y. P.; Zhong, X. J.; Atallah, T. L.; Spencer, M. S.; Brus, L. E.; Jin, S.; Zhu, X. Y. Continuous-Wave Lasing in Cesium Lead Bromide Perovskite Nanowires. *Adv. Opt. Mater.* **2018**, *6* (2), 1700982.
(33) Wu, S.; Liu, Y.; Lin, L.; Chang, Y.; Hsu, H. Characteristics of multi-mode lasing in cesium lead bromide perovskite microwires with an isosceles right triangle cross-section. *Opt. Express* **2021**, *29* (23), 37797−37808.
(34) Wu, Z.; Chen, J.; Mi, Y.; Sui, X.; Zhang, S.; Du, W.; Wang, R.; Shi, J.; Wu, X.; Qiu, X.; Qin, Z.; Zhang, Q.; Liu, X. All-Inorganic CsPbBr3 Nanowire Based Plasmonic Lasers. *Adv. Opt. Mater.* **2018**, *6* (22), 1800674.
(35) Lu, D.; Zhang, Y.; Lai, M.; Lee, A.; Xie, C.; Lin, J.; Lei, T.; Lin, Z.; Kley, C. S.; Huang, J.; Rabani, E.; Yang, P. Giant Light-Emission Enhancement in Lead Halide Perovskites by Surface Oxygen Passivation. *Nano Lett.* **2018**, *18* (11), 6967−6973.
(36) Li, H.; Ai, Q.; Li, Y.; Zhai, X.; Liu, T.; Ren, Y.; Gao, T. Localization of anisotropic exciton polariton condensates in perovskite microcavities. *Appl. Phys. Lett.* **2022**, *120* (1), 011104.
(37) Gao, Y.; Zhao, L.; Shang, Q.; Zhong, Y.; Liu, Z.; Chen, J.; Zhang, Z.; Shi, J.; Du, W.; Zhang, Y.; Chen, S.; Gao, P.; Liu, X.; Wang, X.; Zhang, Q. Ultrathin CsPbX3 Nanowire Arrays with Strong Emission Anisotropy. *Adv. Mater.* **2018**, *30* (31), e1801805.
(38) Bao, W.; Liu, X.; Xue, F.; Zheng, F.; Tao, R.; Wang, S.; Xia, Y.; Zhao, M.; Kim, J.; Yang, S.; Li, Q.; Wang, Y.; Wang, Y.; Wang, L. W.; MacDonald, A. H.; Zhang, X. Observation of Rydberg exciton polaritons and their condensate in a perovskite cavity. *Proc. Natl. Acad. Sci. U. S. A.* **2019**, *116* (41), 20274−20279.
(39) Hu, T.; Xie, W.; Wu, L.; Wang, Y.; Zhang, L.; Chen, Z. Optimized polaritonic modes in whispering gallery microcavities. *Solid State Commun.* **2017**, *262*, 7−10.
(40) Liu, W.; Li, Y.; Yu, H.; Wang, J.; Hu, A.; Jia, S.; Li, X.; Yang, H.; Dai, L.; Lu, G.; Liu, Y.; Wang, S.; Gong, Q. Imaging and Controlling Photonic Modes in Perovskite Microcavities. *Adv. Mater.* **2021**, *33* (25), e2100775.

https://doi.org/10.1021/acs.nanolett.2c03147
Nano Lett. 2022, 22, 9365−9371